Direct conversion of CO2 to dimethyl ether in a fixed bed membrane reactor: Influence of membrane properties and process conditions

Fuel 302 (2021) 121080

Contents lists available at ScienceDirect

Fuel

journal homepage: www.elsevier.com/locate/fuel

Full Length Article

Direct conversion of CO_2 to dimethyl ether in a fixed bed membrane reactor: Influence of membrane properties and process conditions

Serena Poto, Fausto Gallucci, M. Fernanda Neira d'Angelo *

Sustainable Process Engineering, Chemical Engineering and Chemistry, Eindhoven University of Technology, Eindhoven, the Netherlands

ARTICLE INFO

Keywords:
Membrane reactor
CO_2 conversion
DME production
Water removal
Sweep gas

ABSTRACT

The direct hydrogenation of CO_2 to dimethyl ether (DME) is a promising technology for CO_2 valorisation. In this work, a 1D phenomenological reactor model is developed to evaluate and optimize the performance of a membrane reactor for this conversion, otherwise limited by thermodynamic equilibrium and temperature gradients. The co-current circulation of a sweep gas stream through the permeation zone promotes both water and heat removal from the reaction zone, thus increasing overall DME yield (from 44% to 64%). The membrane properties in terms of water permeability (i.e., $4{\cdot}10^{-7}$ mol·Pa^{-1}m^{-2}s^{-1}) and selectivity (i.e., 50 towards H_2, 30 towards CO_2 and CO, 10 towards methanol), for optimal reactor performance have been determined considering, for the first time, non-ideal separation and non-isothermal operation. Thus, this work sheds light into suitable membrane materials for this applications. Then, the non-isothermal performance of the membrane reactor was analysed as a function of the process parameters (i.e., the sweep gas to feed flow ratio, the gradient of total pressure across the membrane, the inlet temperature to the reaction and permeation zone and the feed composition). Owing to its ability to remove 96% of the water produced in this reaction, the proposed membrane reactor outperforms a conventional packed bed for the same application (i.e., with 36% and 46% improvement in CO_2 conversion and DME yield, respectively). The results of this work demonstrate the potential of the membrane reactor to make the CO_2 conversion to DME a feasible process.

1. Introduction

The growing concerns about CO_2 emissions [1,2], and its impact on climate change are driving the research agenda towards more sustainable processes. One of the most powerful solutions to mitigate anthropogenic CO_2 emissions, mostly coming from flue gases of fossil-based power and chemical plants, [5,6]is the carbon capture and storage technology (CCS) [3,4] coupled with the reconversion of the collected CO_2 into valuable products [7–13]. For example, the CO_2 conversion to dimethyl ether (DME) is an intriguing route [7,14]. DME is a clean burning fuel that can replace LPG or diesel without any (or limited) changes in the existing engines [15,16]. When used as a substitute for diesel, DME is particularly attractive due to its high cetane number (i.e., 60), low boiling point (i.e., −2.5 °C), and the lack of C—C bonds [16–18], which render DME an attractive fuel. Currently the synthesis of DME can proceed via two routes. First, the indirect route is based on the initial conversion of syngas to methanol as intermediate product, and its subsequent dehydration to DME. The second route is the direct synthesis of DME from syngas in a single reactor. While the existing technologies for both methanol and DME rely on fossil-based syngas [19,20], leading again to environmental problems [21,22], recent research assesses the prospects of replacing the syngas by CO_2/H_2 feed [7,23], according to the following scheme:

$$\textit{CO}_2\ \textit{hydrogenation}\text{: } CO_2 + 3H_2 \rightleftharpoons CH_3OH + H_2O \quad \Delta H_0 = -49.5\ \text{kJ/mol} \tag{1}$$

$$\textit{Reverse water gas shift: } CO_2 + H_2 \rightleftharpoons CO + H_2O \quad \Delta H_0 = +41.2\ \text{kJ/mol} \tag{2}$$

$$\textit{Methanol dehydration: } 2CH_3OH \rightleftharpoons CH_3OCH_3 + H_2O \quad \Delta H_0 = -23.4\ \text{kJ/mol} \tag{3}$$

The synthesis of methanol (1) is typically carried out over a Cu-ZnO-Al_2O_3 catalyst [24–26], which also activates the water gas shift reaction (2) [27,28]. However, several studies propose novel catalyst formulation with improved performance for the CO_2 hydrogenation to methanol. For example, oxides showing oxygen vacancies (i.e., ZrO_2 or CeO_2) significantly improve the CO_2 activation [29–32].

On the other hand, the methanol dehydration (3) is catalysed by acid catalysts, such as γ-Al_2O_3 or HZSM-5 [33–35]. Several acid catalysts, especially zeolites with different dimensional framework (e.g., FER,

* Corresponding author.
E-mail address: M.F.Neira.dAngelo@tue.nl (M. Fernanda Neira d'Angelo).

https://doi.org/10.1016/j.fuel.2021.121080
Received 8 February 2021; Received in revised form 12 May 2021; Accepted 15 May 2021
Available online 17 June 2021

MOR, MFI) and Si:Al ratios were proposed for the methanol dehydration to DME, where the balance between Bronsted and Lewis acid sites is carefully tuned to selectively dehydrate methanol to DME. The main drawback of these catalysts is their strong hydrophilicity, and consequent deactivation due to strong water adsorption on the acid sites [36–38]. When DME is synthesized via the direct route, the two catalysts are physically mixed to form a bifunctional catalyst [39,35]. Besides the kinetic considerations, the process has important thermodynamic constraints. It is well known that the methanol synthesis is a thermodynamic limited process [40]. Therefore, the immediate consumption of methanol to form DME in the direct route has the beneficial effect of shifting the equilibrium towards higher conversions. Besides, the overall process is exothermic and proceeds with a reduction in the number of moles, so it is thermodynamically favoured at low temperatures and high pressures. Thus, a proper heat management strategy is crucial to prevent hotspots and the consequent conversion losses. Another strategy to overcome thermodynamic limitations is the in situ removal of the large amount of water produced in all individual reactions [41–46]. This is even more important in the direct hydrogenation of CO_2 than in the conventional process starting from syngas, where water is partially consumed by the water gas shift reaction. A promising technologies for the in-situ removal of water is a membrane reactor, where reaction and product separation are coupled to overcome the thermodynamic limitations (*Le Chatelier* principle).

Several studies have been published on the use of both organic and inorganic membranes to enhance the synthesis of methanol. Struis et al. [47,48] showed that the integration of a Nafion membrane for the selective removal of water in a packed bed reactor has remarkable effects on the CO_2 conversion and methanol yield. However, given the poor thermal stability of the polymeric membranes, most of the recent research interests shifted towards inorganic membranes, which are more thermally stable [49–51]. These and other works show that water permeability and selectivity (i.e., H_2O/H_2 and H_2O/CO_2 separation factors) are critical parameters with remarkable impact on the overall process. While the use of membrane technology for the synthesis of methanol is well demonstrated in the literature, and several modelling studies also demonstrate its benefits to enhance the dehydration of methanol to DME [52–54], the application of membrane reactors for the direct conversion of CO_2 to DME (i.e., in one step) has gained research attention only very recently. In fact, the direct synthesis of DME from CO_2-rich syngas (i.e., not yet pure CO_2) became a topic of interests in the last decades due to the popularity of biomass gasification technologies. Several works demonstrated, the importance of the in-situ water removal, especially when gradually replacing CO with CO_2 [42,46,55,56]. De Falco et al. [15,45] showed for the first time that the considerations of a heat management strategy and the operation under non-isothermal conditions are key in this temperature-sensitive process. In view of the increasing interests in CO_2 capture and valorisation, very recently the direct synthesis of DME from concentrated CO_2 and H_2 has become a hot topic. The CO_2-to-DME process is even more challenging than the well-studied (CO_2-rich) syngas route, and thus requires dedicated attention, due to the formation of larger amounts of water, leading to more severe thermodynamic limitations and membrane stability issues.

Very recently, the work of Ateka collaborators [41,44,57], demonstrates the benefits of a packed-bed membrane reactor to boost the synthesis of DME starting from CO_2 and CO mixed in different ratios. Their work considers the use of zeolite membranes (i.e., H-SOD type and LTA type), and concludes that the in-situ removal of water leads to improved DME yields and stable catalytic performance with respect to a conventional packed bed. Nevertheless, their work focuses on relatively high temperature operation (i.e., above 275 °C), which limits the membrane separation performance in terms of water permeability and water separation factors [58]. Although these operating conditions lead to attractive DME yields when starting with CO_2/COx (with COx = CO + CO_2) up to 0.5 (i.e., 65% for pure CO), the reported DME yields for pure CO_2 feeds remain very low (~5%). Thus, it is evident that the shift in feed composition from (CO_2-rich) syngas to pure CO_2 poses additional demands on the membrane separation, and thus requires further investigation. To this end, it is important to consider a wider temperature range (i.e., especially towards lower temperatures that favour water permeation), as well as the non-ideal behaviour of real membranes. Most of the modelling studies reported so far [15,45,46,55,56], including the most recent works by Ateka et al. [44], consider zeolite membranes that ideally permeate only the smallest molecules (i.e., H_2O and H_2). However, the likely permeation of other gases such as CO and methanol may significantly reduce the DME yield, and therefore should be taken into account when optimizing membrane properties. Furthermore, the importance of the heat integration in this process should not be underestimated, as temperature enormously affects the product distribution (i.e., reactions limited by thermodynamic equilibrium), as well as the membrane separation properties and stability. Indeed, if an adequate strategy to control the temperature gradients is not adopted, the process would converge into the r-WGS [59].

In this study, we describe the performance of a membrane reactor for the direct conversion of CO_2 to DME through a non-isothermal phenomenological 1D reactor model. We propose a reactor configuration in which a sweep gas is fed co-currently with the feed to promote both water and heat removal from the reaction zone. This work does not focus on a specific membrane material, but rather aims at identifying the required membrane properties (i.e., permeability and selectivity of all the species) which maximize DME yield and CO_2 conversion, and uses that as a basis for the identification of a suitable membrane material. Among the available membrane materials, this work pays special attention to porous membranes as they fulfil important prerequirements concerning hydrophilicity, thermal and mechanical stability and high selectivity [43]. The effect of process parameters (i.e., the sweep gas to feed flow ratio, the gradient of total pressure across the membrane, the inlet temperature to the reaction and permeation zone and the feed composition) on CO_2 conversion and DME selectivity is investigated through parametric studies. Finally, this work provides insights about optimal membrane properties and process conditions that render maximum DME yields.

2. Reactor configuration and modelling

2.1. Description of the reactor configuration

In this work we consider the fixed bed membrane reactor sketched in Fig. 1, with the properties summarized in Table 1. It is composed of two coaxial tubes: an inner tubular membrane and an outer reactor shell which hosts the catalyst bed, giving raise to two zones, referred as the permeation and the reaction zone, respectively. This configuration allows for a high mechanical stability of the membrane, and easy optimization of the ratio between the membrane area and catalyst volume. Since the permeation of species depends on the gradient in partial pressure across the membrane, two different approaches can be considered to promote the removal of water: 1) applying a gradient of total pressure between the reaction and the permeation zone; and 2) feeding a sweep gas through the permeation zone to dilute the permeated water. The first solution leads to more mechanical stress on the membrane, and a higher driving force for the permeation of all the species, leading to the unwanted loss of reactants. On the other hand, using a sweep gas with the same composition of the feed favours the selective removal of water and minimizes reactants loss. In this study, a sweep gas is fed in a cocurrent configuration in order to enhance water removal at the beginning of the reactor, where the reaction rate and water formation are the highest. Additionally, the cocurrent circulation of the sweep gas at a lower temperature favours the removal of the heat of the reaction, optimizing the temperature profile. For an exothermic reaction, a cocurrent circulation of the reaction mixture and the cooling fluid is preferred, because most of the heat is produced at the beginning

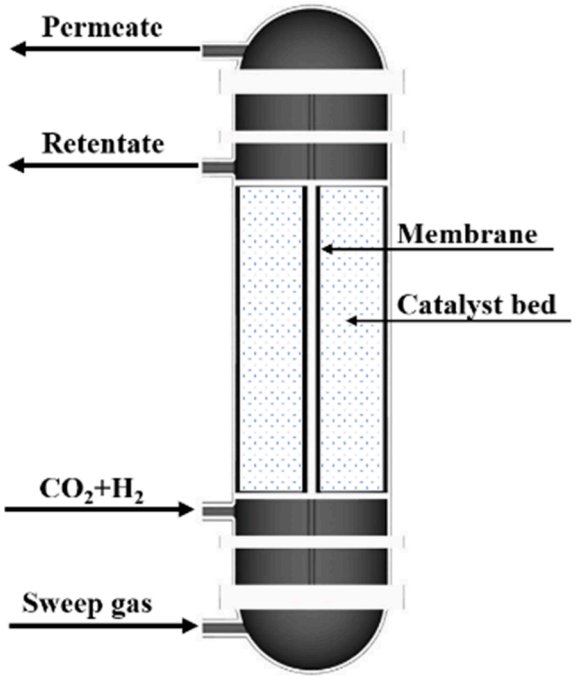

Fig. 1. Schematic representation of the packed bed membrane reactor.

Table 1
Main characteristics of the fixed bed membrane reactor.

Parameter	Value
Reactor shell internal diameter, D_{si} (m)	0.0198
Bed and membrane length, L (m)	1
Catalyst particle diameter, d_p (m)	$4{\cdot}10^{-4}$
Catalyst density, ρ_c (kg/m^3)	1982
Bed porosity, ε (−)	0.4
External membrane diameter, D_{mo} (m)	$14{\cdot}10^{-3}$
Internal membrane diameter, D_{mi} (m)	$10{\cdot}10^{-3}$

of the reactor.

2.2. Modelling equations

The phenomenological reactor model relies on the following assumptions:

1. Steady state conditions
2. 1D ideal plug flow (i.e., axial and radial dispersion is neglected by considering L/dp $\geq$ 50 and D/dp $\geq$ 25, respectively)
3. Kinetic control regime (i.e., the solid and gas phase are described as a single pseudo-homogeneous phase, due to the absence of mass transfer limitations)
4. Negligible pressure drops in the permeation side
5. Kinetics by Lu et al. [60] valid for conventional and membrane reactor
6. Inert membrane material under reaction conditions.

Accordingly, the membrane reactor model consists of mass and energy balances for both the reaction and permeation zone, and a momentum balance for the reaction zone only. For each of the six chemical species that take part in the process (i), the following equations hold:

$$\frac{dF_i^R}{dz} = \rho_c(1-\varepsilon)\sum_{j=1}^{N_r}\left(r_j\nu_{ji}\right)\frac{\pi}{4}\left(D_{si}^2 - D_{mo}^2\right) - J_i\pi D_{mo} \tag{4}$$

$$\frac{dF_i^P}{dz} = J_i\pi D_{mo} \tag{5}$$

where J_i is the flux of component i through the membrane, as defined in Eq. (6). By definition, J_i is positive when the species permeates from the reaction to the permeation zone.

$$J_i = \wp_i\cdot\left(P_i^R - P_i^P\right) \tag{6}$$

$\wp_i$ is the permeance of the component i and P_i^R and P_i^P are its partial pressure in the reaction and permeation zone, respectively. The selectivity of water with respect to the component i is defined as follows:

$$S_{H_2O/i} = \frac{\wp_{H_2O}}{\wp_i} \tag{7}$$

In this work, the dependency of $\wp_i$ on the composition was neglected because the composition of water (i.e., the primarily permeating species) does not change significantly, as confirmed later in Section 3.3. In addition, it is assumed that the permeation flux is limited by the transport trough the membrane selective layer. Indeed, gas permeation is usually not affected by concentration polarization phenomena (i.e., resistance to the transport from a bulk phase to the membrane surface) because of the high diffusivity and low permeability of the gases, when compared to liquids [61].

In this work, we consider the kinetic model by W. Lu et al. (Eq. (8)–(10)) for the well-studied $CuZnOAl_2O_3$/HZSM-5 bifunctional catalyst [60]. The extensive amount of experimental data reported for such catalyst allow us to easily validate the kinetic model, as well as its implementation into our reactor model. Nevertheless, other kinetic models have been reported in literature [60,62–68], very recently also for new catalyst types, such as CuO-ZnO-MnO/SAPO-18 [69] and a core shell $CuOZnOZrO_2$@SAPO-18 [70].

Coke formation and water adsorption (i.e. main causes of catalyst deactivation) are avoided due to the relatively low reaction temperatures and the water removal, respectively. The rate expressions derive from a Langmuir Hinshelwood model, in which the water and methanol adsorption on the catalyst surface are neglected.

$$r_1 = k_1\frac{P_{CO_2}P_{H_2}\left(1 - \frac{1}{K_{p,1}}\frac{P_{H_2O}P_{CH_3OH}}{P_{CO_2}{P_{H_2}}^3}\right)}{\left(1 + K_{CO_2}P_{CO_2} + K_{CO}P_{CO} + \sqrt{K_{H_2}P_{H_2}}\right)^3} \tag{8}$$

$$r_2 = k_2\frac{\frac{1}{K_{p,2}}\frac{P_{CO_2}P_{H_2}}{P_{CO}} - P_{H_2O}}{\left(1 + K_{CO_2}P_{CO_2} + K_{CO}P_{CO} + \sqrt{K_{H_2}P_{H_2}}\right)} \tag{9}$$

$$r_3 = k_3\left(\frac{{P_{CH_3OH}}^2}{P_{H_2O}} - \frac{P_{CH_3OCH_3}}{K_{p,3}}\right) \tag{10}$$

Here P_i is the partial pressure of each component in the reaction zone, calculated as the product between the total pressure and the molar fractions. The kinetics [60], adsorption [71,72] and equilibrium constants [72] are shown in Table 2.

The energy balance in the reaction and the permeation zone are described in Eqs. (11) and (12), respectively. These balances assume heat exchange between the reaction and permeation zone, but the reactor is isolated from the external environment to evaluate the thermal effects of feeding cold sweep gas as single cooling strategy.

$$\sum_{i=1}^{N_s}\left(F_i^R cp_i\right)\frac{dT^R}{dz} = \rho_c(1-\varepsilon)\frac{\pi}{4}\left(D_{si}^2 - D_{mo}^2\right)\sum_{j=1}^{N_r} r_j\left(-\Delta H_r\left(T^R\right)\right) + \\ -U\pi D_{mi}\left(T^R - T^P\right) - \pi D_{mo}\Sigma_{(i=1)}^{(N_s)}\Sigma\left(J_i cp_i\left(T^R - T_{mr}\right)\right) \tag{11}$$

$$\sum_{i=1}^{N_s}\left(F_i^P cp_i\right)\frac{dT^P}{dz} = U\pi D_{mi}\left(T^R - T^P\right) + \pi D_{mo}\sum_{i=1}^{N_s}\left(J_i cp_i\left(T_{mp} - T^P\right)\right) \tag{12}$$

Table 2
Kinetic parameters of the catalytic hydrogenation of CO_2 to DME.

Kinetic parameter	Value
k_1	$35.45exp\left(-\frac{1.7609\cdot10^4}{RT}\right) kmol/\left(kg_{cat}\cdot s\cdot bar^2\right)$
k_2	$7.3976exp\left(-\frac{2.0436\cdot10^4}{RT}\right) kmol/\left(kg_{cat}\cdot s\cdot bar\right)$
k_3	$8.2894\cdot10^4 exp\left(-\frac{5.2940\cdot10^4}{RT}\right) kmol/\left(kg_{cat}\cdot s\cdot bar\right)$
K_{H_2}	$0.249exp\left(\frac{3.4394\cdot10^4}{RT}\right) 1/bar$
K_{CO_2}	$1.02\cdot10^{-7}exp\left(\frac{6.74\cdot10^4}{RT}\right) 1/bar$
K_{CO}	$7.99\cdot10^{-7}exp\left(\frac{5.81\cdot10^4}{RT}\right) 1/bar$
$K_{p,1}$	$\exp(4213/T - 5.752\cdot ln(T) - 1.707\cdot10^{-3}T + 2.682\cdot10^{-6}T^2 - 7.232\cdot10^{-10}T^3 + 17.6)$
$K_{p,2}$	$\exp(2167/T - 0.5194\cdot log(T) + 1.037\cdot10^{-3}T - 2.331\cdot10^{-7}T^2 - 1.277)$
$K_{p,3}$	$\exp(4019/T + 3.707\cdot ln(T) - 2.783\cdot10^{-3}T + 3.8\cdot10^{-7}T^2 - 6.56\cdot10^4/T^3 - 26.64$

The global heat transfer coefficient U describes three consecutive heat transfer phenomena: 1) the convection in the inner tube, 2) the conduction trough the membrane and 3) the convection in the outer tube.

$$\frac{1}{U} = \frac{1}{h_{mi}} + \frac{D_{mi}}{2}\frac{1}{k_m} ln\left(\frac{D_{mo}}{D_{mi}}\right) + \frac{D_{mi}}{D_{mo}}\frac{1}{h_{mo}} \quad (13)$$

The heat transfer coefficient in the permeation zone (h_{mi}) and reaction zone (h_{mo}) are calculated according to the correlations by Dittus-Boelter [73] and Li-Finlayson [74], respectively (details in SI). The temperature at the membrane surface on the reaction (T_{mr}) and permeation side (T_{mp}) are determined by the steady state energy balance around the membrane.

$$\left(T_{mp} - T^P\right) h_{mi}\frac{D_{mi}}{2} = \frac{\left(T_{mr} - T_{mp}\right)k_m}{ln\left(\frac{D_{mo}}{D_{mi}}\right)} \quad (14)$$

$$\left(T_{mp} - T^P\right) h_{mi} D_{mi} = \left(T^R - T_{mr}\right) h_{mo} D_{mo} \quad (15)$$

The momentum balance in the reaction zone is described by the Ergun equation (Eq. (16)), while the pressure drop along the permeation zone is considered negligible.

$$\frac{dP^R}{dz} = \frac{150\mu(1-\varepsilon)^2 v}{\varepsilon^3 d_p^2} + \frac{1.75(1-\varepsilon)\rho v^2}{\varepsilon^3 d_p} \quad (16)$$

The above set of equations are implemented in MATLAB R2019a and solved numerically with the *ode15s* function.

2.3. Operating conditions and parametric studies

Two parametric studies were performed to determine the optimal membrane properties (i.e., $\wp_{H_2O}$ and $S_{H_2O/i}$ in the range summarized in Table 3) that render maximum CO_2 conversion and DME yield. The first parametric study (P1) assumes that only the smallest molecules (i.e., H_2O and H_2) permeates through the membrane, while the other species do not permeate (i.e., ideal membrane assumption). This initial study is used to determine the optimal values $\wp_{H_2O}$ and S_{H_2O/H_2}. The second parametric study (P2) considers a real membrane where all species may permeate, and it is used to find the optimal selectivity of water with respect to the remaining species. Both P1 and P2 were carried out assuming isothermal conditions, and thus the membrane properties refer to the chosen temperature.

Table 3
Range of $\wp_{H_2O}$ and $S_{H_2O/i}$ for the parametric studies (P1 and P2).

Membrane property	P1 – ideal membrane	P2 – real membrane
$\wp_{H_2O}$(mol·Pa^{-1}m^{-2}s^{-1})	0–1·10^{-6}	Optimal value from P1
S_{H_2O/H_2} (–)	0.5–50	Optimal value from P1
S_{H_2O/CO_2} (–)	∞	5–50
$S_{H_2O/CO}$ (–)	∞	5–50
$S_{H_2O/MeOH}$ (–)	∞	5–10
$S_{H_2O/DME}$ (–)	∞	∞

The ranges of $\wp_{H_2O}$ and $S_{H_2O/i}$ considered in P1 and P2 are summarized in Table 3. Typical values of $\wp_{H_2O}$ for porous membranes reported in the literature vary from 6.8·10^{-8} to 9.7·10^{-8} mol·Pa^{-1}m^{-2}s^{-1}[46]. Thus, this study assess the effect of $\wp_{H_2O}$ between 0 and 1·10^{-6} mol·Pa^{-1}m^{-2}s^{-1}. With respect to the remaining species, we consider that water will likely condense in the meso and micro-pores of the membrane due to the low capillary pressures (e.g., capillary pressure = 10 bar at 200 °C for a pore size of 1 nm in a hydrophilic membrane). This will effectively reduce the pore size, and, consequently, hinder the permeation of non-condensable gases. Therefore, for most cases water has the highest permeance (i.e., $>1 S_{H_2O/i}$). Nevertheless, values of S_{H_2O/H_2} lower than 1 were also considered in this study due to contemplate the possibility of competitive permeation of these two species, with very similar size. In the worst case scenario (i.e., separation dictated by the Knudsen diffusion, usually occurring at higher temperatures within the bigger pores [75]), the Knudsen perm-selectivity of water and H_2 is $S_{H_2O/H_2} = \sqrt{\frac{M_{wH_2}}{M_{wH_2O}}} = 0.33$. Thus, the minimum value of S_{H_2O/H_2} is set to 0.5 (i.e., around 50% higher than the Knudsen perm-selectivity value), although this type of flow is not likely within a hydrophilic membrane. Data from literature [76,77] show that CO and CO_2 permeances are very similar, due to their comparable molecular size. For this reason, the H_2O/CO_2 and H_2O/CO selectivity was set at the same value. Next, the permeance of methanol is higher than those of non-condensable gases (i.e., $S_{H_2O/MeOH}$ is lower) because methanol may also permeate through capillary condensation. Finally, DME cannot condense under reaction conditions because it exceeds its critical temperature (128 °C) under the operating conditions. DME molecular size is the largest among all the species in this process, which justifies the assumption of an infinite H_2O/DME selectivity. The kinetic diameter of all the species are reported in the SI. The dissolution of species in the condensed water was assumed negligible in this study, since liquid water only exists inside the (small) pore volume.

Table 4 reports the operating conditions evaluated in this study. These were kept constants during P1 and P2, while a third parametric study (P3) aimed to assess the effect of some operating conditions, within the range reported in Table 4, on the reactor performance. An average temperature of 200 °C was set as the target within the reaction zone in order to: 1) avoid catalyst deactivation, which occurs at

Table 4
Operating conditions adopted in the simulations.

Operating condition	P1	P2	P3
H_2:CO_2, (mol/mol)[a]	3	3	3–10
$\Phi^R_{H_2,0}$ (Nm^3/h)	0.1	0.1	0.1
T^R_0(K)	473	473	473
T^P_0(K)	473	473	393–473
P^R_0, (bar)	40	40	40
ΔP (bar)[b]	0	0	0–40
SW (–)[c]	**3**	**3**	3–50

[a] The composition of the feed to the reaction and permeation zone is the same.

[b] ΔP is the gradient in total pressure across the membrane.

[c] SW is the sweep gas to feed molar flow ratio.

temperatures greater than 270–300 °C [60,78,79]; 2) limit the production of CO, which occurs preferentially at elevated temperatures; 3) guarantee a sufficiently fast water permeation trough the membrane, which is enhanced at lower temperatures due to its transport mechanism [80,81]; and 4) guarantee sufficient catalyst activity, which demands temperatures greater than 190–200 °C [82]. Finally, a total pressure of 40 bar was set in the reaction zone.

The reactor performance was evaluated in terms of CO_2 conversion, product yield and selectivity, and the amount of water removed. The loss or cofeeding of reactants (i.e., through back-permeation of sweep gas in the reaction zone) was considered in the following definitions [83]:

$$X_{CO_2} = \frac{F^R_{CO_2,0} - F^R_{CO_2} + F_{CO_2,tmb}}{F^R_{CO_2,0} + F^*_{CO_2,tmb}} \tag{17}$$

$$Y_i = \frac{N_{c,i}\left(F^R_i + F^P_i\right)}{F^R_{CO_2,0} + F^*_{CO_2,tmb}} \tag{18}$$

$$S_i = \frac{Y_i}{X_{CO_2}} \tag{19}$$

$$F_{CO_2,tmb} = F^P_{CO_2,0} - F^P_{CO_2} CO2\ transmembrane\ flow \tag{20}$$

$$F^*_{CO_2,tmb} = 0\ if\ F_{CO_2,tmb} \leq 0 Reactant\ loss \tag{21}$$

$$F^*_{CO_2,tmb} = F_{CO_2,tmb}\ if\ F_{CO_2,tmb} > 0\ Reactant\ cofeeding \tag{22}$$

$$WR = \frac{F^P_{H_2O}}{F^P_{H_2O} + F^R_{H_2O}} \tag{23}$$

where $N_{c,i}$ is the number of carbon atoms in the considered species. The *WR* is an important key performance indicator, that represents the membrane efficiency. This variable was introduced by Battersby et al. [84], who defined the product of the Peclet and Damkohler numbers (*DaPe*) as a new dimensionless number representing the combined effect of reaction and separation. According to the *DaPe* definition (Eq. (25)), a membrane reactor works in optimal conditions when *DaPe* approaches unity, which means, in our process, that all the water produced is removed trough the membrane. However, $DaPe = 1$ describes a thermodynamic limit that can only be approached. Therefore, when *DaPe* exceeds 1, water builds-up in the reactor, indicating a poor performance of the membrane reactor.

$$DaPe = \frac{Maximum\ reaction\ rate\ per\ unit\ volume}{Maximum\ permeation\ rate\ per\ unit\ volume} \tag{24}$$

In this work, the *WR* number represents the reciprocal of the *DaPe* number.

3. Simulation results and discussion

This section discusses the validation of the kinetic model and the results of the parametric studies for the optimization of the membrane properties (i.e., P1 and P2) and the process conditions (P3).

3.1. Validation of the kinetic model

The validity of our model was assessed by reproducing the experimental results of Ren et al. [85] derived for a $CuZnOAl_2O_3$/HZSM-5 bifunctional catalyst in a packed bed reactor, where the two functions were mixed in a 1:1 wt ratio. In Fig. 2 the results of the simulation related to both CO_2 conversion and DME yield are compared with the experimental data at a pressure of 28 bar, a GHSV of 1215 $NL/(kg_{cat}\cdot h)$ and a H_2/CO_2 molar ratio of 3:1. The model fits quite well the experimental data at lower temperatures (i.e., T ≤ 250 °C), which is the T range in which Lu et al. [60] studied the kinetics. Therefore, predictions beyond this T range have not been performed in this study. At 220 °C, the divergence between the model prediction and the experimental data is 1.92% for CO_2 conversion, 3.5% for DME yield and 1.05% for CO yield. The difference between the experimental data and the simulated values, which is larger at higher temperature, derives from the different composition of the catalytic bed of the two mentioned studies. However, the kinetic model describes the experimental trend with temperature of both CO_2 conversion and DME yield.

Furthermore, the correct implementation of the kinetics was assessed by reproducing the theoretical results of a conventional packed bed reactor by Iliuta et al. [55] (see Fig. S2 of SI), with a deviation lower than 2%.

3.2. Optimization of membrane properties ($\wp_{H_2O}$ and $S_{H_2O/i}$)

3.2.1. Results of parametric studies

In this section, we first optimized the $\wp_{H_2O}$ and S_{H_2O/H_2} using the parametric study P1 (i.e., ideal membrane hypothesis holds), since they do not depend on the permeation of the other species. Fig. 3a shows the effect of $\wp_{H_2O}$ on the water transmembrane flow, which expectedly

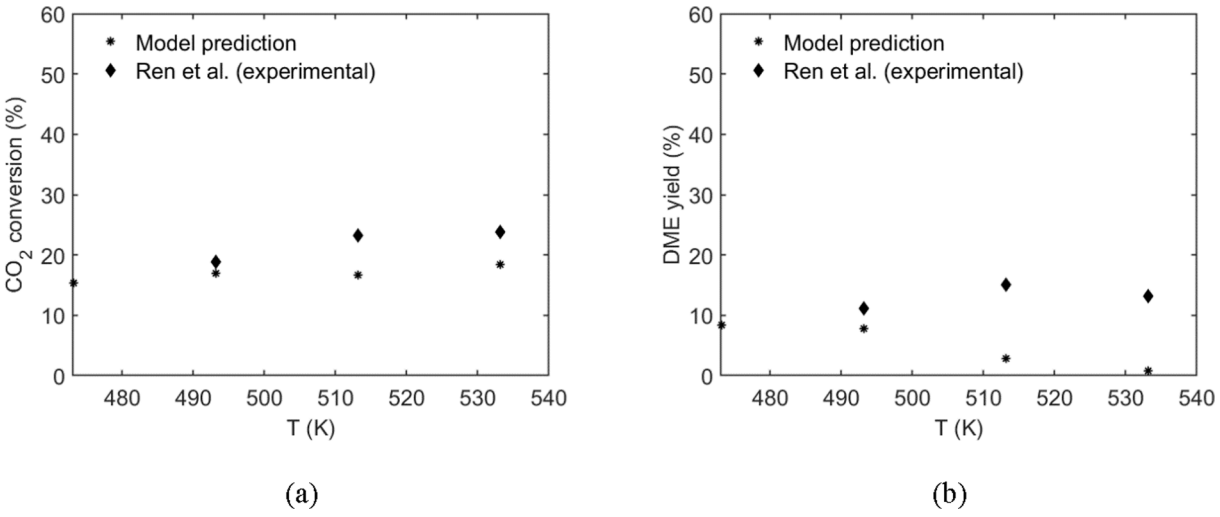

Fig. 2. Comparison between the experimental data of Ren et al. [85] and the data obtained with the model prediction for a conventional reactor: CO_2 conversion (a) and DME yield (b) as a function of temperature at 28 bar, GHSV of 1215 $NL/(kg_{cat}\cdot h)$ and H_2/CO_2 molar ratio at 3:1.

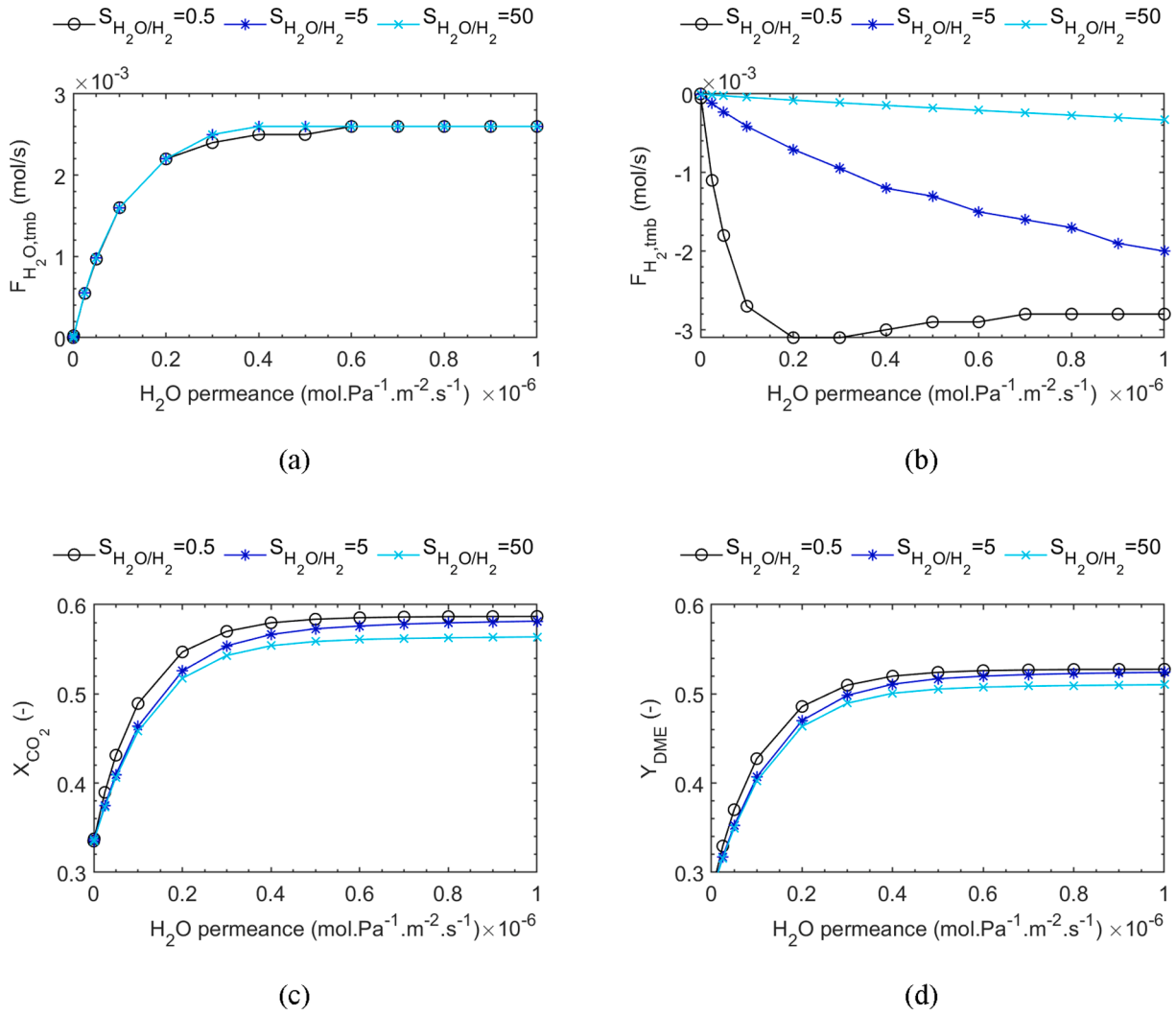

Fig. 3. Effect of the H_2O permeance and H_2O/H_2 selectivity on the membrane reactor performances in terms of: a) water transmembrane flow ($F_{H_2O,tmb}$), b) hydrogen transmembrane flow ($F_{H_2,tmb}$), c) CO_2 conversion (X_{CO_2}) and d) DME yield (Y_{DME}). In each plot, curves are parametric for the H_2O/H_2 selectivity (Se).

increases with greater permeances, reaching a plateau at around $4{\cdot}10^{-7}$ mol/(Pa·m^2·s), where the thermodynamic equilibrium between the reaction and the permeation zone is established. Accordingly, increasing permeance leads to improvement on CO_2 conversion (Fig. 3c) and DME yield (Fig. 3d) up to 0.6 and 0.5, respectively, due to a shift in the thermodynamic equilibrium.

In addition, Fig. 3 shows the effect of the selectivity of water with respect to H_2 on the same performance indicators (i.e., transmembrane flow of water and H_2, and resulting CO_2 conversion and DME yield). The ideal membrane allows only water and hydrogen to permeate. In principle, an increase in S_{H_2O/H_2} may be considered advantageous to promote the permeation of water with respect to that of H_2 (i.e., a valuable reactant). Loosing H_2 through the membrane would be detrimental for the final DME yield as well as for the economics of the process. In this case, however, the composition of the sweep and feed gas streams are the same, which in facts results in a net back permeation of H_2 from the permeation to the reaction zone regardless of the selectivity. This phenomenon, hereby referred as cofeeding, explains the negative values reported in Fig. 3b, particularly at low S_{H_2O/H_2} values (i.e., poorly selective membranes). In other words, there is no need for a highly selective membrane to prevent H_2 loss when using a sweep gas with the same concentration as the feed mixture.

As shown in Fig. 3b and c, H_2 cofeeding is beneficial both for the CO_2 conversion and DME yield, in line with the work of Diban et al. [46]. Interestingly, our results also show that decreasing the H_2O/H_2 selectivity by three orders of magnitude leads to a negligible effect on the reactor performance. The low sensitivity of the process to variations in membrane selectivity is conducive to a very robust reactor concept. However, excessive cofeeding is undesirable because it would require a significant H_2 reintegration in the sweep gas before its recycle. In other words, despite the negligible effects of the perm-selectivity of hydrogen on conversion and yields, it is desirable that the membrane preferentially enhances the separation of water (i.e., relatively high values of S_{H_2O/H_2}). In that case, the permeated water can be easily condensed from the outlet of the permeation zone, facilitating direct recirculation of the sweep gas without complex post processing units. Thus, a S_{H_2O/H_2} of 50 was considered for the rest of this study.

Afterwards, we optimized the $S_{H_2O/CO}$, S_{H_2O/CO_2} and $S_{H_2O/MeOH}$ with the parametric study P2, which considers a real membrane. Fig. 4a shows the effect of the H_2O/CO_x selectivity (where CO_x refers to either CO_2 or CO, with assumed equal permeance) on CO_2 conversion and products yield. Both CO_2 conversion and DME yield display a very mild increase with greater H_2O/CO_x selectivity, up to a maximum value of 0.60 and 0.42, respectively. On the other hand, methanol and CO yield are nearly unaffected by the H_2O/CO_x selectivity. In principle, increasing the H_2O/CO_x selectivity has two main advantages: 1) both the loss and cofeeding of CO_2 is limited, requiring no adjustment of the CO_2 composition in the sweep gas prior to recirculation, and 2) CO

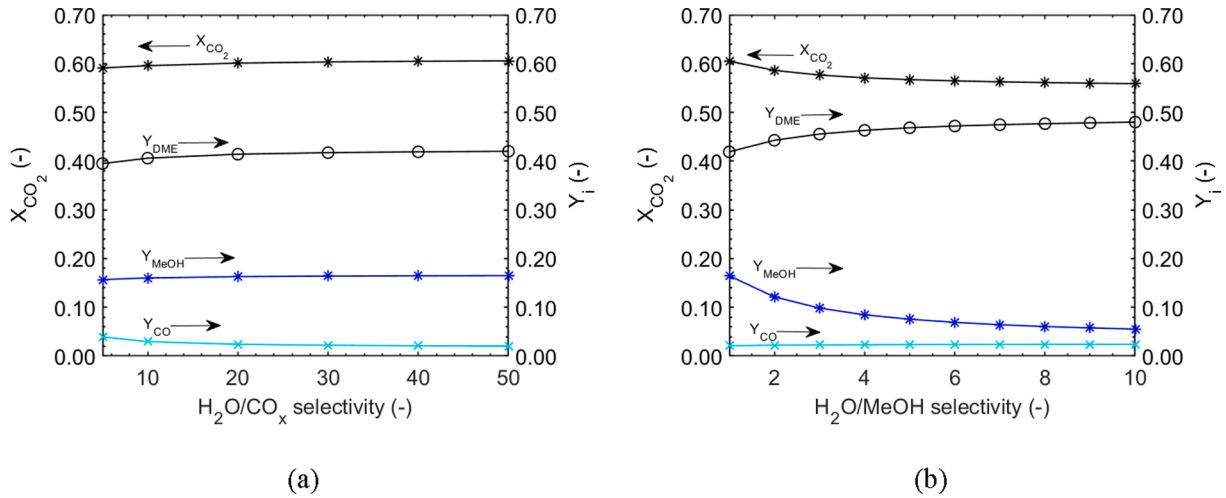

Fig. 4. Effect of the H_2O/CO_x (a) and H_2O/MeOH selectivity (b) on the membrane reactor performances in terms of CO_2 conversion (X_{CO_2}), DME yield (Y_{DME}), methanol yield (Y_{MeOH}) and CO yield (Y_{CO}).

permeation is limited, which minimizes the extent of the reverse water gas shift reaction and thereby improves DME selectivity. However, these results show that the susceptibility of the system to this parameter is negligible, due to the use of a sweep gas with equal concentration as the feed stream, which limits the gases permeation in both ways. Hence, an average value 30 (i.e., a value in the middle of the range explored) is used in the rest of this study.

Fig. 4b shows a slight negative effect of H_2O/MeOH selectivity on the CO_2 conversion and methanol yield. Expectedly, a greater methanol permeation (i.e., a low selectivity) results in a shift in the thermodynamic equilibrium of the CO_2 hydrogenation reaction (i.e., reaction (1)). In this process, such situation is not desired since methanol permeation will limit its further dehydration to DME. For the same reason, when increasing the H_2O/MeOH selectivity, DME yield increases. Likewise in previous cases, the DME yield does not seem very sensitive to a 10 fold increase in the H_2O/MeOH selectivity. Further, Fig. 4b shows that this selectivity has no effect on the CO yield, as expected. Since a higher value of selectivity is not physically expected, the optimal value of H_2O/MeOH selectivity is set to 10.

Finally, the large kinetic diameter of DME and its non-condensable nature under reaction conditions justifies the assumption of infinite H_2O/DME selectivity. However, it should be noted that an infinite value for the H_2O/DME selectivity is not necessarily optimal, since the removal of DME from the reaction environment is expected to enhance its production. However, it would also require the recovery of DME from the permeate stream. This would demand additional equipment and energy intensive DME/CO_2 downstream separation track.

Table 5 summarises the optimal membrane permeability properties as determined in the previous parametric studies (P1-P2).

3.2.2. Discussion on suitable membrane materials

Based on the results of the parametric studies, we elucidate on a suitable membrane material for the conversion of CO_2 to DME. To allow the separation of water vapor from a mixture of gases (e.g., H_2 and CO_2) the selected membrane material should be porous and possess affinity to water (i.e., it should be hydrophilic), thus favouring the permeation of water through capillary condensation and hindering that of non-condensable gases. The exact pore size of such material may be tailored as a trade-off between permeation fluxes and selectivity, which will strongly depend on the material itself and its degree of hydrophilicity. Besides its permeation properties, the membrane material should also be mechanically and thermo-chemically stable under process conditions. This is, the membrane should withstand pressures of 10–50 bar and temperature of 200–300 °C in humid environments, while preserving its chemical and porous structure, and associated permeation properties.

Polymeric membranes display adequate separation performance, but they undergo degradation at temperatures above their glass transition point (i.e., usually below 200 °C) and swelling phenomena may occur in too humid environment. The second important category of membranes material are porous ceramic membranes [86,87] (e.g., alumina, silica, zirconia, titania or a mixture of them). Among them, zeolite membranes have been widely studied for pervaporation [88]. Indeed, several works describe the potential of microporous zeolite membranes for the selective removal of water for different processes such as the methanol synthesis [43,49–51], the Fischer Tropsch process [83,77] and the DME synthesis as well [41,42,44–46,56,57]. Table 6 reports the properties of zeolite membranes in terms on $\wp_{H_2O}$ and $S_{H_2O/i}$ we retrieved from a literature survey. Although the reported permeation properties of zeolite membranes look very promising and match with our requirements, their

Table 5
Optimal membrane properties determined through the parametric studies.

Estimated membrane performance	Value
H_2O permeance, $\wp_{H_2O}$ (mol·Pa^{-1}m^{-2}s^{-1})	$4{\cdot}10^{-7}$
H_2O/H_2 selectivity, S_{H_2O/H_2} (−)	50
H_2O/CO_2 selectivity, S_{H_2O/CO_2} (−)	30
H_2O/CO selectivity, $S_{H_2O/CO}$ (−)	30
H_2O/MeOH selectivity, $S_{H_2O/MeOH}$ (−)	10
H_2O/DME selectivity, $S_{H_2O/DME}$ (−)	∞

Table 6
Summary of the literature review on the properties of zeolite membranes in terms on $\wp_{H_2O}$ and $S_{H_2O/i}$, in the temperature range of 200–250 °C.

Parameter	Value	Reference
H_2O permeance, $\wp_{H_2O}$ (mol·Pa^{-1}m^{-2}s^{-1})	$6.8{\cdot}10^{-8}$–$1{\cdot}10^{-6}$	[51,58,98–55,59,77,92–97]
H_2O/H_2 selectivity, S_{H_2O/H_2} (−)	2–50	[51,58,77,93–95,98,99,101,55]
H_2O/CO_2 selectivity, S_{H_2O/CO_2} (−)	2.45–17.7	[77,100,102,103,104]
H_2O/CO selectivity, $S_{H_2O/CO}$ (−)	3.7–19.6	[77,100,102,103,104]
H_2O/MeOH selectivity, $S_{H_2O/MeOH}$ (−)	1–9	[58,92,96,99,105,106]
H_2O/DME selectivity, $S_{H_2O/DME}$ (−)	Not defined	–

stability in hot humid environments remains a topic of concern within the experimental research [89]. Their high separation factors, especially at high temperature, are still under investigations. In addition, it is difficult to obtain a large crack free zeolite membrane [90,91].

Carbon molecular sieve membranes (CMSM) are another interesting category of inorganic porous membranes that could be suitable for this application. Carbon membranes derive from the pyrolysis of a polymeric precursor [107], and according to the conditions of the carbonization process, different groups of atoms are removed from the precursor. The residual functional groups are responsible for the membrane hydrophilicity. Besides, these membranes are stable in both humid and hot environment, as far as the carbonization temperature (e.g. typically above 400 °C) is not overcome. Even if the concept of carbon membranes can be found back in the early 1970 [107], they have only been tested for gas separation processes [108,109]. Experimental results regarding this last category of membranes, especially concerning the permeation of condensable species, are not available yet. Therefore, further investigation is required. Owing to its promising features, however, the following section considers the membrane module as an alumina supported carbon molecular sieve membrane [110].

3.3. Optimization of the operating conditions

This section discusses the effect of the main operating conditions on the reactor performance. In these simulations, the reactor is no longer considered isothermal. The heat balances are solved by considering an alumina supported carbon molecular sieve membrane material [110] for the membrane module, in line with the previous discussion. The conductivity of this material is calculated in SI. The permeance and selectivity values of the selected membrane are shown in Table 5.

3.3.1. Effect of the sweep gas to feed flow ratio (SW) and the gradient of total pressure (ΔP)

The sweep gas to feed flow ratio (SW) and the gradient of total pressure across the membrane (ΔP) are the main parameters regulating the transmembrane driving force. Fig. 5a, b and c show the effect of SW and ΔP on CO_2 conversion, DME yield and water removal (WR), which all increase when both SW and ΔP increase, up to an asymptotic value of 0.63, 0.53 and 0.96, respectively. An increase in both SW and ΔP effectively decreases the partial pressure of water in the permeate zone, and thus increases the driving force for water removal (i.e., greater WR). Therefore, the CO_2 conversion and DME yield, which benefit from the removal of water due to thermodynamic reasons, show the same trend as WR.

All the variables describing the reactor performance reach an asymptotic value when increasing SW and ΔP. In particular, the percentage of water removed from the reaction zone approaches a value slightly lower than 1 (i.e., between 0.94 and 0.96), indicating that most

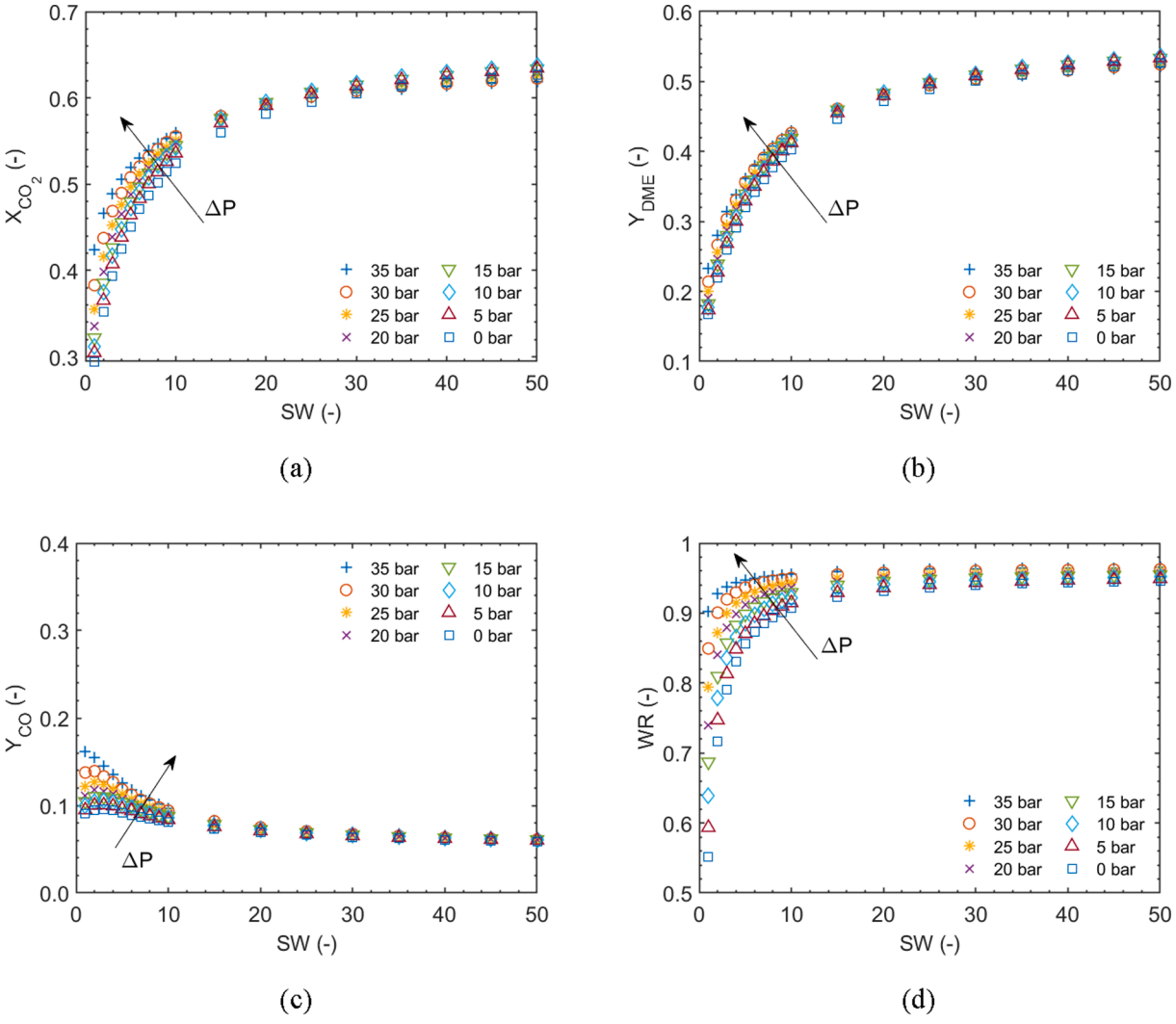

Fig. 5. Effect of the SW ratio and the ΔP on the reactor performances in terms of a) CO_2 conversion (X_{CO_2}), b) DME yield (Y_{DME}), c) CO yield (Y_{CO}) and d) water removal (*WR*), (H_2:CO_2 = 3; T_0^p = 473 K, all the other process conditions are reported in Table 4 – P3).

of the water produced in the reaction is effectively removed from the reaction zone. However, complete water removal is not possible due to the thermodynamic equilibrium established between the reaction and permeation zone.

It is interesting to note that WR, and accordingly CO_2 conversion and DME yield, are particularly sensitive to SW, while the effects of ΔP are less significant, especially at high SW. For example, for a SW of 50, an increase of ΔP from 0 to 40 bar leads to the mild increase in CO_2 conversion and DME yield from 0.62 to 0.63 and from 0.52 to 0.53 respectively. On the other hand, increasing the ΔP, also leads to the undesired loss of reactants or methanol. This is minimized by adjusting the composition of the sweep gas and tuning the membrane properties (i.e., increasing the $S_{H_2O/MeOH}$). These findings are in line with similar results reported in literature [46,55,56,83]. Furthermore, Gorbe et al [51] reported a decrease in the water/gas separation factors for higher temperatures and ΔP related to the same reason. Therefore, the membrane properties and the compression costs required for the sweep gas will dictate the final choice of ΔP. Since this cost analysis is outside the scope of this study, a value of 5 bar for the ΔP was assumed for the following study.

Fig. 5c shows the effect of SW and ΔP on CO yield. Upon increasing SW at constant ΔP, CO yield goes through a maximum and then decreases to reach a plateau. The CO transmembrane flow (shown in Fig. S5 of SI) shows the same behaviour. Initially absent in the sweep gas stream, both CO and water permeate through the membrane, enhancing the formation of CO via the reverse WGS reaction. Above a certain value of SW – which is lower as higher is the ΔP – the effect of water removal on the methanol synthesis and dehydration reaction becomes more significant. Likewise the previous trends and following analogous rationale, the CO yield also benefits from increasing ΔP. The ΔP effect on the CO yield is negligible, especially for high values of SW. The asymptotic value of CO yield is 0.06, showing that the DME selectivity is very high under these conditions.

In the proposed reactor concept, the sweep gas also acts as a cooling fluid that helps minimize temperature gradients. The temperature profile of the reaction zone along the reactor shows the typical trend of an exothermic reaction, when a colder fluid – in this case the sweep gas – is circulated in cocurrent mode. The temperature increases up to a maximum (i.e., hot spot) and then decreases to reach an asymptotic value. Therefore, we can identify two characteristic temperatures: 1) the maximum temperature (T^R_{max}) and 2) the asymptotic temperature (T^R_{end}). Fig. 6 shows the effect of SW and ΔP on T^R_{max} and T^R_{end}. While $T^R_{max}$is nearly independent on SW, the use of sweep gas seems to be an effective strategy to minimize T^R_{end}. An increase in the SW ratio (i.e., increase the sweep gas flow rate and velocity) increases the heat transfer coefficient (see correlations in SI), improving the heat removal capacity of the sweep gas itself. Besides, larger values of SW lead to higher water transmembrane flows, which contributes to the heat removal as well.

As expected, the ΔP shows no influence on the temperature profile, since it does not influence nor the water transmembrane flow or the heat removal related to convection.

According to these results, we can conclude that for a SW greater than 20 there is no significant improvement in the reactor performance and most of the variables reach their asymptotic value (i.e., an increase of SW from 20 to 30 leads to an insignificant improvement in CO_2 conversion and DME yield lower than 5% and only 1% decrease in T^R_{end}). As mentioned earlier, an average temperature of 200 °C in the rection zone was selected as a compromise between the reaction kinetics, thermodynamics, catalyst stability and the water separation considerations. Therefore, the sweep gas inlet temperature was adjusted accordingly. The final temperature, T^R_{end}, reaches a value of 200 °C when T^P_0 is 185 °C, confirming that the sweep gas, in these conditions, has a sufficient heat removal capacity to optimize the reactor temperature profile (see Fig. S7 of SI).

3.3.2. *Effect of feed composition*

A key constraint for the methanol and DME production from CO_2 + H_2 mixtures is the need of large amounts of expensive H_2. In fact, a large H_2:CO_2 molar ratio favours the CO_2 hydrogenation reactions, both from the kinetic and thermodynamic point of view. Fig. 7 shows the effect of the H_2:CO_2 molar ratio on DME yield for either a conventional and a membrane reactor. It is clear that a high H_2 concentrations increases the DME yields for both the membrane reactor (up to about 0.7) and for a conventional one (up to about 0.4), but it comes at the expense of high operational costs. Thus, a proper optimization of this parameter should result from an economic evaluation. Here, the membrane reactor offers a clear economic advantage to the conventional packed bed reactor, as it achieves greater DME yields, and importantly, it reaches its maximum DME yields at lower H_2:CO_2 ratio.

On the other hand, the membrane reactor configuration we propose, utilizes a CO_2 + H_2 stream as sweep gas, with a *SW* ratio of 20. Such stream contributes only to water and heat removal, thus it could be recirculated back to the reactor with a ≈100% recycle ratio. Fig. 8 shows the concentration profile of the sweep gas along the reactor. As expected, the main components of this stream are CO_2 and H_2, with minor amounts of the reaction products (see zoomed in profiles in Fig. 8b). The molar fractions of CO_2 and H_2 in the permeation zone suffer from negligible changes along the reactor. Therefore, the sweep gas can be

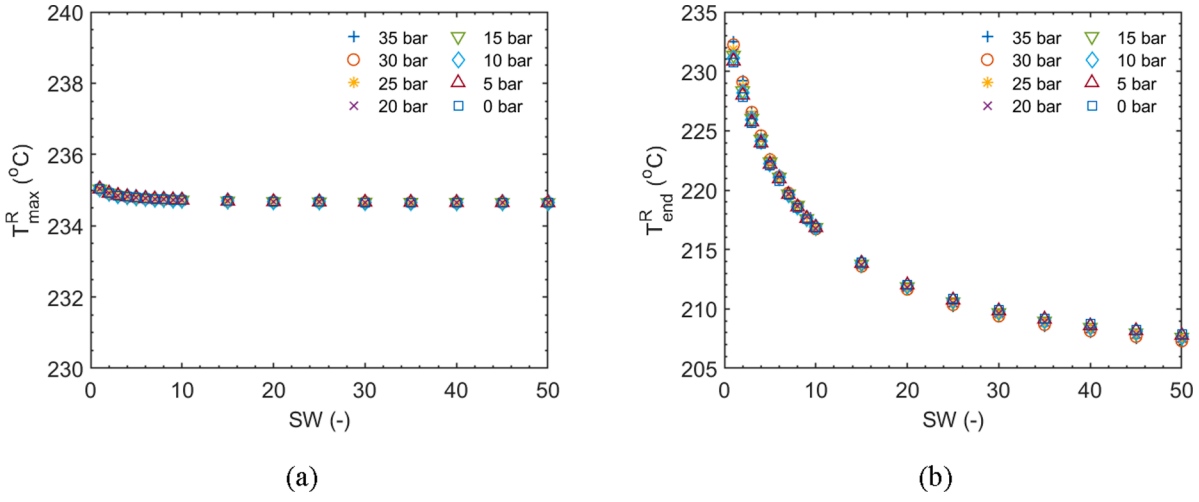

Fig. 6. Effect of the SW ratio and the ΔP on the reaction zone temperature profile: a) temperature (T^R_{max}) as a function of the SW ratio and ΔP; b) the asymptotic temperature value (T^R_{end}) as a function of the SW ratio and ΔP (H_2:CO_2 = 3; T^P_0 = 473 K, all the other process conditions are reported in Table 4 – P3).

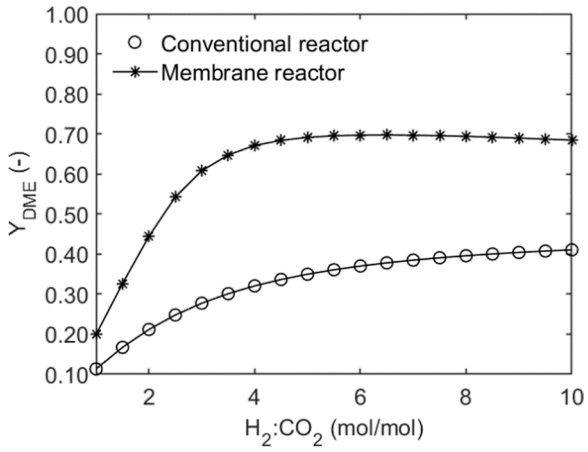

Fig. 7. Effect of the inlet H_2:CO_2 molar ratio on the DME yield (Y_{DME}) for a membrane reactor with a SW = 20; ΔP = 5 bar; T^R_{avg} = 473 K (all the other process conditions are reported in Table 4 – P3) and a conventional reactor working at the same conditions in terms of total pressure (i.e., 40 bar) and average temperature (i.e., 473 K).

recycled to the reactor after limited post treatments (i.e., condensation of the permeated water and a make-up of CO_2 and H_2 of 0.13% and 0.0038% of the initial flow rate, respectively). Water is the only species that significantly permeates along the reactor, reaching a WR of 96%. Even then, its concentration in the permeation zone is very low, confirming that the circulation of a sweep gas generates sufficient driving force for water permeation by diluting water in this stream, even if the gradient of total pressure is close to zero. The sweep gas at the outlet of the reactor contains also a small amount of CO (0.018%) and methanol (0.028%), which can be recycled together with CO_2 and H_2. The presence of methanol and CO in the sweep gas will further avoid the undesired permeation of these species from the reaction side.

3.4. Optimized membrane reactor performance vs thermodynamic limitations

This section discusses the performance of the optimized membrane reactor and compares it with the thermodynamic limitations. The optimal operating conditions for the membrane reactor are summarised in Table 7. Fig. 9 shows the profiles of the main reactor variables (i.e., T^R, T^P, $y^R_{H_2O}$, $y^P_{H_2O}$, X_{CO_2}, Y_{DME}) as a function of the reactor length (z). The temperature profile (Fig. 9a) shows the role of the sweep gas as a cooling agent which minimizes axial temperature profiles in the reaction zone. The water concentration in the reaction zone remains very low along the reactor, which confirms that the membrane reactor has reached its target, with an efficiency of water separation of 96% (see *WR* profile in Fig. S8b of SI). In addition, Fig. 9a also shows that the peak of water concentration is near the reactor inlet, reassuring the choice the cocurrent operation. Since the reaction rate is the highest in the beginning of the reactor, both heat and water production are maximum at this point. Therefore, in this zone the highest driving force for both the heat and water removal is required.

The pressure drops in the reaction zone are lower than 0.1 bar, under these conditions (see Fig. S8a of SI). This is important to minimize compression costs and to prevent back-permeation of water at the end of the reactor. Fig. 9b shows the membrane reactor performance in terms of CO_2 conversion and DME yield and demonstrate that this reactor configuration clearly overcomes the thermodynamic limitation under these conditions. Fig. 9b shows that CO_2 conversion and DME yield exceed the thermodynamic values (i.e., best possible performance of a conventional packed bed reactor) by 36.4% and 43.3%, respectively. This result proves that the selective removal of water in a membrane reactor strongly enhances both the methanol production and its dehydration to DME. Therefore, we believe that the use of membrane reactor technology will be key to increase the feasibility of the direct conversion of CO_2 to DME.

Finally, Fig. 10 underlines the importance of the heat management in this process by comparing the temperature profiles considering the proposed heat management solution with the corresponding temperature profile under adiabatic conditions. The latter shows a first temperature rise of around 50–60 °C, followed by a decrease in temperature due to the thermodynamically favoured endothermic r-WGS reaction.

Table 7
Optimal operating conditions for the membrane reactor.

Operating condition	Value
Reaction zone inlet temperature, T^R_0 (K)	473
Permeation zone inlet temperature, T^P_0 (K)	458
Reaction zone pressure, P^R (bar)	40
Pressure difference across the membrane, ΔP (bar)	5
Sweep gas to feed flow ratio, SW (−)	20
H_2:CO_2 molar feed ratio (both zones)	3.5
Inlet volumetric flow of H_2 in the reaction zone, $\Phi^R_{H_2,0}$ (Nm^3/h)	0.1

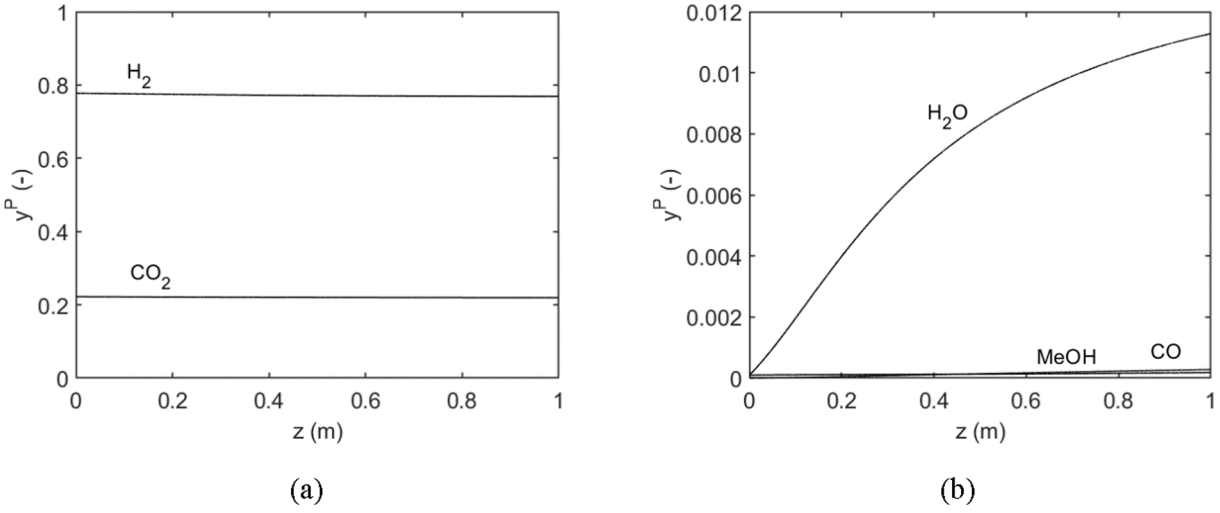

Fig. 8. Sweep gas (or permeation zone gaseous mixture) concentration profile of a) the main component of the streams (CO_2 and H_2) and b) the permeating species (H_2O, CH_3OH and CO).

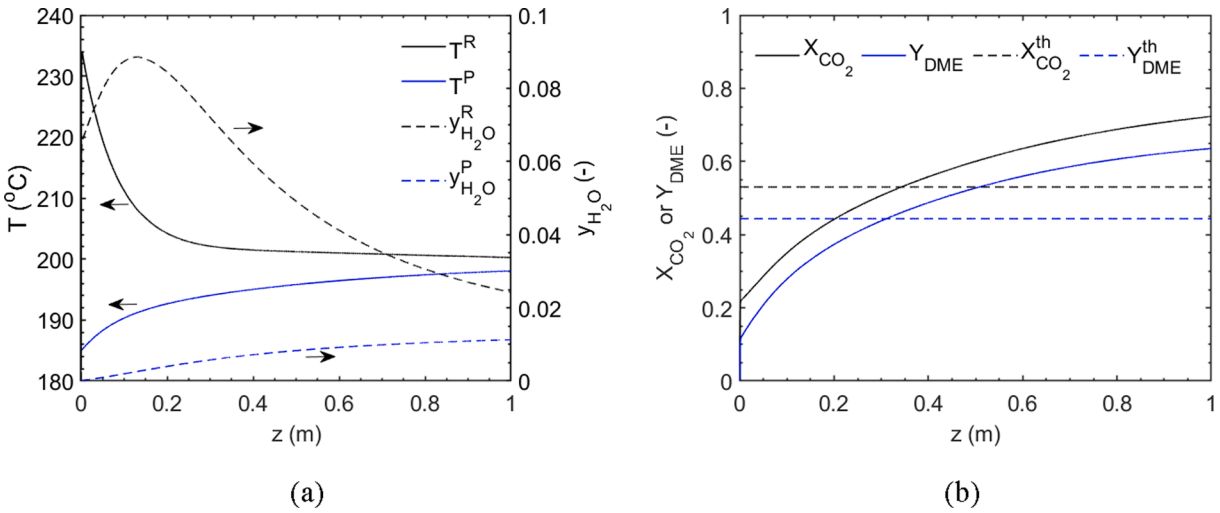

Fig. 9. Membrane reactor performance: a) temperature and water molar fraction profiles; b) CO_2 conversion and DME yield profile, together with the respective thermodynamic limitations ($X^{th}_{CO_2}$ and Y^{th}_{DME}), calculated at 40 bar and 200 °C. The membrane reactor operating conditions are reported in Table 6).

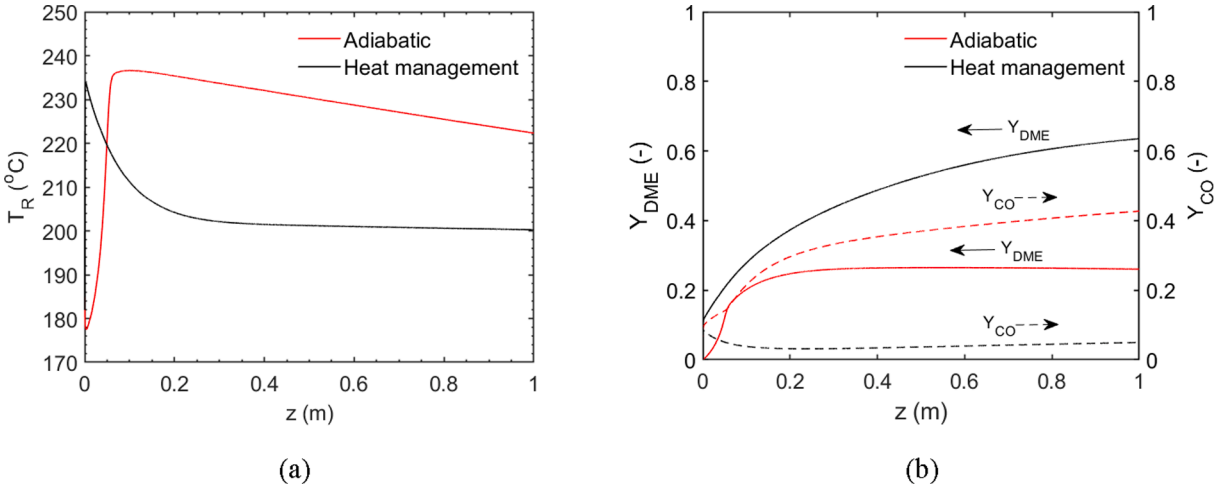

Fig. 10. Comparison of the membrane reactor performance in adiabatic conditions (red lines) and with the heat management strategy proposed in this work (black lines), in terms of: a) temperature profile in the reaction zone and b) DME yield (solid line) and CO yield (dashed line). The membrane reactor operating conditions are reported in Table 6. (For interpretation of the references to colour in this figure legend, the reader is referred to the web version of this article.)

This temperature profile leads to greater CO yield, as shown in Fig. 10b (i.e., CO yield increases from 0.05 to 0.43, whilst DME yield decreases from 0.63 to 0.26).

4. Conclusions

This work demonstrates the possibility of upgrading CO_2 for the production of dimethyl ether, which is an attractive alternative fuel with low environmental impact. We developed a non-isothermal 1D phenomenological reactor model to evaluate and optimize the performance of a membrane reactor for this conversion, otherwise limited by thermodynamic equilibrium and temperature gradients. We first showed the credibility of the modelling approach, by reproducing experimental results retrieved from literature. Afterwards, we studied the effect of the membrane properties on the reactor performance and accordingly identified a suitable membrane material for this process. We conclude that the optimal membrane for this process should have a water permeance of c.a. $4{\cdot}10^{-7}$ mol·Pa^{-1}m^{-2}s^{-1}, a water perm-selectivity of 50 towards H_2, 30 towards CO_2 and CO, 10 towards methanol and a very large perm-selectivity toward DME, so that its permeation may be neglected. Among the available membrane materials, zeolites show suitable performance, but may pose stability problems under reaction conditions. Carbon membranes, on the other hand, seem promising.

The circulation of a sweep gas ($SW = 20$) in cocurrent mode proved an effective strategy to minimize hot spots and temperature gradients as well as to enhance water removal while avoids water back permeation.

We underlined the importance of the heat integration in this process, where temperature gradients could enormously affect the product distribution, moving the reactions toward undesired pathways (i.e., production of CO).

The SW ratio showed a higher influence on the reactor performances than the gradient of the total pressure (ΔP), lowering the demands on the membrane mechanical stability. We also showed that the integration of a membrane for the selective water removal in a conventional packed bed reactor lowers the H_2 requirement that maximizes the DME yield, which is key for the industrial attractiveness of the process. With optimal membrane properties and optimal process conditions, the membrane reactor technology shows its potential to overcome the severe thermodynamic limitations of this process. In particular, if 96% of the water produced by the reactions is removed, the CO_2 conversion and DME yield show an improvement of 36% and 43% each, with respect to a

conventional packed bed reactor working at the same operating conditions (i.e., 200 °C and 40 bar).

Our results show the possibility to easily integrate this reactor in a conventional process scheme, since the sweep gas does not require complex post processing units in order to be recirculated in the permeation zone.

CRediT authorship contribution statement

Serena Poto: Methodology, Conceptualization, Software, Investigation, Validation, Writing - original draft, Writing - review & editing. **Fausto Gallucci:** Investigation, Supervision, Project administration, Writing - review & editing. **M. Fernanda Neira d'Angelo:** Investigation, Supervision, Project administration, Writing - review & editing.

Declaration of Competing Interest

The authors declare that they have no known competing financial interests or personal relationships that could have appeared to influence the work reported in this paper.

Acknowledgements

This project has received funding from the European Union's Horizon 2020 research and innovation programme under grant agreement No 838014 (*C2Fuel* project).

Appendix A. Supplementary data

Supplementary data to this article can be found online at https://doi.org/10.1016/j.fuel.2021.121080.

References

[1] Tucker M. Carbon dioxide emissions and global GDP. Ecol Econ 1995;15(3):215–23.
[2] Yu CH, et al. A review of CO2 capture by absorption and adsorption. Aerosol Air Quality Res 2012;12.5:745–69.
[3] Albo J, Luis P, Irabien A. Carbon dioxide capture from flue gases using a cross-flow membrane contactor and the ionic liquid 1-ethyl-3-methylimidazolium ethylsulfate. Ind Eng Chem Res 2010;49(21):11045–51.
[4] Figueroa JD, Fout T, Plasynski S, McIlvried H, Srivastava RD. Advances in CO2 capture technology-The U.S. Department of Energy's Carbon Sequestration Program. Int J Greenh Gas Control 2008, 2008,;2(1):9–20.
[5] Rubin ES, Davison JE, Herzog HJ. The cost of CO2 capture and storage. Int J Greenhouse Gas Control 2015;40:378–400.
[6] Steeneveldt R, Berger B, Torp TA. CO2 capture and storage: Closing the knowing-doing gap. Chem Eng Res Des 2006;84(9):739–63.
[7] Pontzen F, Liebner W, Gronemann V, Rothaemel M, Ahlers B. CO2-based methanol and DME – Efficient technologies for industrial scale production. Catal Today 2011;171(1):242–50.
[8] De Vasconcelos Miguel, Carlos Eduardo Gerardes, "CO2 capture and valorisation to chemicals: methane production," 2018.
[9] Chery D, Lair V, Cassir M. Overview on CO2 valorization: Challenge of molten carbonates. Front Energy Res 2015;2015(3):1–10.
[10] Zhang Z, Hu S, Song J, Li W, Yang G, Han B. Hydrogenation of CO2 to formic cid promoted by a diamine-functionalized ionic liquid. ChemSusChem 2009;2(3):234–8.
[11] Yang H, Kaczur JJ, Sajjad SD, Masel RI. Electrochemical conversion of CO2 to formic acid utilizing Sustainion™ membranes. J CO2 Util 2017;20:208–17.
[12] Khan MMT, Halligudi SB, Shukla S. Reduction of CO2 by molecular hydrogen to formic acid and formaldehyde and their decomposition to CO and H2O. J Mol Catal 1989;57(1):47–60.
[13] Kuhl KP, Hatsukade T, Cave ER, Abram DN, Kibsgaard J, Jaramillo TF. Electrocatalytic conversion of carbon dioxide to methane and methanol on transition metal surfaces. J Am Chem Soc 2014;136(40):14107–13.
[14] Ma J, et al. A short review of catalysis for CO2 conversion. Catal Today 2009;148(3-4):221–31.
[15] De Falco M, Capocelli M, Centi G. Dimethyl ether production from CO2 rich feedstocks in a one-step process: Thermodynamic evaluation and reactor simulation. Chem Eng J 2016;294:400–9.
[16] Japar SM, et al. Ozone-Forming Potential of a series of oxygenated organic compounds. Environ Sci Technol 1991;25:415–20.
[17] Arcoumanis C, Bae C, Crookes R, Kinoshita E. The potential of di-methyl ether (DME) as an alternative fuel for compression-ignition engines: a review. Fuel 2008;87(7):1014–30.
[18] S. Tosaka, Y. Fujiwara and T. Marayaman, "The effect of fuel properties on particulate formation (the effect of molecular structure and carbon number)" Automot. News, 1988.
[19] Lv Y, Wang T, Wu C, Ma L, Zhou Y. Scale study of direct synthesis of dimethyl ether from biomass synthesis gas. Biotechnol Adv 2009;27(5):551–4. https://doi.org/10.1016/j.biotechadv.2009.04.005.
[20] Phienluphon R, et al. Designing core (Cu/ZnO/Al2O3)-shell (SAPO-11) zeolite capsule catalyst with a facile physical way for dimethyl ether direct synthesis from syngas. Chem Eng J 2015;270:605–11.
[21] van Dyk JC, Keyser MJ, Coertzen M. Syngas production from South African coal sources using Sasol-Lurgi gasifiers. Int J Coal Geol 2006;65(3–4):243–53.
[22] Rath LK, Longanbach JR. A perspective on syngas from coal. Energy Sources 1991;13(4):443–59.
[23] Catizzone E, Bonura G, Migliori M, Frusteri F, Giordano G. CO2 recycling to dimethyl ether: State-of-the-art and perspectives. Molecules 2018;23(1):1–28.
[24] Bowker M, Hadden RA, Houghton H, Hyland JNK, Waugh KC. The mechanism of methanol synthesis on copper/zinc oxide/alumina catalysts. J Catal 1988;109(2):263–73.
[25] Himelfarb PB, Simmons GW, Klier K, Herman RG. Precursors of the copper-zinc oxide methanol synthesis catalysts. J Catal 1985;93(2):442–50.
[26] Waugh KC. Methanol Synthesis. Catal Today 1992;15(1):51–75.
[27] Edwards JF, Schrader GL. Infrared spectroscopy of Cu/ZnO catalysts for the water-gas shift reaction and methanol synthesis. J Phys Chem 1984;88(23):5620–4.
[28] Rhodes C, Hutchings GJ, Ward AM. Water-gas shift reaction: finding the mechanistic boundary. Catal Today 1995;23(1):43–58.
[29] Jadhav SG, et al. Catalytic carbon dioxide hydrogenation to methanol: a review of recent studies. Chem Eng Res Des 2014;92(11):2557–67.
[30] Liu XM, et al. Recent Advances in Catalysts for Methanol Synthesis via Hydrogenation of CO and CO2. Ind Eng Chem Res 2003;42(25):6518–30.
[31] Ateka A, et al. Performance of CuO–ZnO–ZrO2 and CuO–ZnO–MnO as metallic functions and SAPO-18 as acid function of the catalyst for the synthesis of DME co-feeding CO2. Fuel Process Technol 2016;152:34–45.
[32] Shi Z, Tan Q, Wu D. Ternary copper-cerium-zirconium mixed metal oxide catalyst for direct CO2 hydrogenation to methanol. Mater Chem Phys 2018;219:263–72.
[33] Jiang S, et al. Dehydration of Methanol to Dimethyl Ether over ZSM-5 Zeolite. Bull Korean Chem Soc 2004;25(2):185–9.
[34] Mollavali M, et al. Intrinsic kinetics study of dimethyl ether synthesis from methanol on γ-Al2O3 catalysts. Ind Eng Chem Res 2008;47(9):3265–73.
[35] Bonura G, et al. Catalytic behaviour of a bifunctional system for the one step synthesis of DME by CO 2 hydrogenation. Catal Today 2014;228:51–7.
[36] Hosseininejad S, Afacan A, Hayes RE. Catalytic and kinetic study of methanol dehydration to dimethyl ether. Chem Eng Res Des 2012;90(6):825–33.
[37] Jun KW, et al. Catalytic dehydration of methanol to dimethyl ether (DME) over solid-acid catalysts. Bull Korean Chem Soc 2002;23(6):803–6.
[38] Bonura G, et al. Acidity control of zeolite functionality on activity and stability of hybrid catalysts during DME production via CO2 hydrogenation. J CO2 Util 2017;24:398–406.
[39] Frusteri F, et al. Multifunctionality of Cu-ZnO-ZrO2/H-ZSM5 catalysts for the one-step CO2-to-DME hydrogenation reaction. Appl Catal B Environ 2015;162:57–65.
[40] Balint, "Margarines and Shortenings IAN," Ullmann's Encycl. Ind. Chem., 2005, 12: 413–454.
[41] Rodriguez-Vega P, et al. Experimental implementation of a catalytic membrane reactor for the direct synthesis of DME from H2+CO/CO2. Chem Eng Sci 2021;234(116396).
[42] Farsi M, Hallaji Sani A, Riasatian P. Modeling and operability of DME production from syngas in a dual membrane reactor. Chem Eng Res Des 2016;112:190–8.
[43] F. Gallucci, Inorganic Membrane Reactors for Methanol Synthesis. Elsevier B.V., 2018.
[44] Ateka A, Ereña J, Bilbao J, Aguayo AT. Strategies for the Intensification of CO2 Valorization in the One-Step Dimethyl Ether Synthesis Process. Ind Eng Chem Res 2020;59(2):713–22.
[45] De Falco M, Capocelli M, Basile A. Selective membrane application for the industrial one-step DME production process fed by CO2 rich streams: Modeling and simulation. Int J Hydrogen Energy 2017;42(10):6771–86.
[46] Diban N, et al. Influence of the membrane properties on the catalytic production of dimethyl ether with in situ water removal for the successful capture of co 2. Chem Eng J 2013;234:140–8.
[47] Struis RPWJ, Stucki S, Wiedorn M. A membrane reactor for methanol synthesis. J Memb Sci 1996;113(1):93–100.
[48] Struis RPWJ, Stucki S. Verification of the membrane reactor concept for the methanol synthesis. Appl Catal A Gen 2001;216(1–2):117–29.
[49] Gallucci F, Paturzo L, Basile A. An experimental study of CO2 hydrogenation into methanol involving a zeolite membrane reactor. Chem Eng Process Process Intensif 2003;43(8):1029–36.
[50] Gallucci F, Basile A. A theoretical analysis of methanol synthesis from CO2 and H2 in a ceramic membrane reactor. Int J Hydrogen Energy 2007;32(18):5050–8.
[51] Gorbe J, et al. Preliminary study on the feasibility of using a zeolite A membrane in a membrane reactor for methanol production. Sep Purif Technol 2017;200:164–8.
[52] Fedosov DA, Smirnov AV, Shkirskiy VV, Voskoboynikov T, Ivanova II. Methanol dehydration in NaA zeolite membrane reactor. J Memb Sci 2015;486:189–94.
[53] Volkov VV, et al. Catalytic conversion of methanol to dimethyl ether on polymer/ceramic composite membranes. Catal Today 2012;193(1):31–6.
[54] Brunetti A, et al. Methanol Conversion to Dimethyl Ether in Catalytic Zeolite Membrane Reactors. ACS Sustain Chem Eng 2020;8(28):10471–9.

[55] Iliuta I, Larachi F, Fongarland P. Dimethyl ether synthesis with in situ H2o removal in fixed-bed membrane reactor: Model and simulations. Ind Eng Chem Res 2010;49(15):6870–7.
[56] Diban N, et al. Improved performance of a PBM reactor for simultaneous CO2 capture and DME synthesis. Ind Eng Chem Res 2014;53(50):19479–87.
[57] Ateka A, et al. Model validation of a packed bed LTA membrane reactor for the direct synthesis of DME from CO/CO2. Chem Eng J October 2020;408.
[58] Rohde MP, Schaub G, Khajavi S, Jansen JC, Kapteijn F. Fischer-Tropsch synthesis with in situ H2O removal - Directions of membrane development. Microporous Mesoporous Mater 2008;115(1–2):123–36.
[59] J. Lee, et al., "Low-temperature CO2 hydrogenation overcoming equilibrium limitations with polyimide hollow fiber membrane reactor," Chem. Eng. J., vol. 403, no. July 2020.
[60] W. Lu, L. Teng, and W. Xiao, "Simulation and experiment study of dimethyl ether synthesis from syngas in a fluidized-bed reactor," 2004, 59: 5455–5464.
[61] Giacinti Baschetti M, De Angelis MG. "Vapour permeation modelling", *Pervaporation, Vapour Permeation and Membrane Distillation*. Woodhead Publishing 2015:203–46.
[62] An X, Zuo YZ, Zhang Q, Wang DZ, Wang JF. Dimethyl ether synthesis from CO2 hydrogenation on a CuO-ZnO-Al2O3-ZrO2/HZSM-5 bifunctional catalyst. Ind Eng Chem Res 2008;47(17):6547–54.
[63] Ng KL, Chadwick D, Toseland BA. Kinetics and modelling of dimethyl ether synthesis from synthesis gas. Chem Eng Sci 1999;54(15–16):3587–92.
[64] Nie Z, Liu H, Liu D, Ying W, Fang D. Intrinsic kinetics of dimethyl ether synthesis from syngas. J Nat Gas Chem 2005;14(1):22–8.
[65] Park N, Park MJ, Lee YJ, Ha KS, Jun KW. Kinetic modeling of methanol synthesis over commercial catalysts based on three-site adsorption. Fuel Process Technol 2014;125:139–47.
[66] Shim HM, Lee SJ, Yoo YD, Yun YS, Kim HT. Simulation of DME synthesis from coal syngas by kinetics model. Korean J Chem Eng 2009;26(3):641–8.
[67] Aguayo AT, Ereña J, Mier D, Arandes JM, Olazar M, Bilbao J. Kinetic modeling of dimethyl ether synthesis in a single step on a CuO-ZnO-Al2O3/γ-Al2O3 catalyst. Ind Eng Chem Res 2007;46(1):5522–30.
[68] Behloul CR, Commenge JM, Castel C. Simulation of reactors under different thermal regimes and study of the internal diffusional limitation in a fixed-bed reactor for the direct synthesis of dimethyl ether from a CO2-Rich input mixture and H2. Ind Eng Chem Res 2021;60(4):1602–23.
[69] A. Ateka J. Ereña J. Bilbao A.T. Aguayo Kinetic modeling of the direct synthesis of dimethyl ether over a CuO-ZnO-MnO/SAPO-18 catalyst and assessment of the CO2 conversion Fuel Process. Technol. 181 2018 no. September, pp. 233–243.
[70] A. Ateka M. Sánchez-Contador A. Portillo J. Bilbao A.T. Aguayo Kinetic modeling of CO2+CO hydrogenation to DME over a CuO-ZnO-ZrO2@SAPO-11 core-shell catalyst Fuel Process. Technol. 206 2020 no. February, p. 106434.
[71] Vanden Bussche KM, Froment GF. A steady-state kinetic model for methanol synthesis and the water gas Shift reaction on a commercial Cu/ZnO/Al2O3 catalyst. J Catal 1996;161(1):1–10.
[72] Zhang DY, Cao HT, Fang FHLiuDH. Thermodynamic analysis for synthesis of dimethyl ether and methanol from synthesis gas. J ECUST 2001;27:198–201.
[73] Taler D, Taler J. Simple heat transfer correlations for turbulent tube flow. E3S Web Conf 2017;13:1–7.
[74] C. Engmeermg, Heat Transfer in Packed Beds. 1976.
[75] J. A. Medrano, et al., "Transport mechanism and modeling of microporous carbon membranes", Current Trends and Future Developments on (Bio-) Membranes.. Elsevier 2019, 39-58.
[76] Rafael L. Espinoza et al., "Production of Hydrocarbons", United States Patent No US-6403600-B1, Jun.11, 2002.
[77] Espinoza RL, Du Toit E, Santamaria J, Menendez M, Coronas J, Irusta S. Use of membranes in Fischer-Tropsch reactors. Stud Surf Sci Catal 2000;130(1):389–94.
[78] Twigg MV, Spencer MS. Deactivation of copper metal catalysts for methanol decomposition, methanol steam reforming and methanol synthesis. Top Catal 2003:191–203.
[79] Kung HH. Deactivation of methanol synthesis catalysts - a review. Catal Today 1992;11(4):443–53.
[80] Okamoto KI, et al. Zeolite NaA membrane: preparation, single-gas permeation, and pervaporation and vapor permeation of water/organic liquid mixtures. Ind Eng Chem Res 2001;40(1):163–75.
[81] Sommer S, Melin T. Influence of operation parameters on the separation of mixtures by pervaporation and vapor permeation with inorganic membranes. Part 1: dehydration of solvents. Chem Eng Sci 2005;60(16):4509–23.
[82] Bukhtiyarova M, et al. Methanol synthesis from industrial CO2 sources: a contribution to chemical energy conversion. Catal Letters 2017;147(2):416–27.
[83] Rohde MP, Unruh D, Schaub G. Membrane application in fischer-tropsch synthesis to enhance CO2 hydrogenation. Ind Eng Chem Res 2005;44(25):9653–8.
[84] Battersby S, et al. An analysis of the Peclet and Damkohler numbers for dehydrogenation reactions using molecular sieve silica (MSS) membrane reactors. Catal Today 2006;116(1):12–7.
[85] Ren S, et al. Highly active and selective Cu-ZnO based catalyst for methanol and dimethyl ether synthesis via CO2 hydrogenation. Fuel 2019;239:1125–33.
[86] Amin SK, et al. An overview of production and development of ceramic membranes. Int J Appl Eng Res 2016;11(12):7708–21.
[87] Lee KP, Arnot TC, Mattia D. A review of reverse osmosis membrane materials for desalination-Development to date and future potential. J Memb Sci 2011;370(1–2):1–22.
[88] Wee SL, Tye CT, Bhatia S. Membrane separation process-Pervaporation through zeolite membrane. Sep Purif Technol 2008;63(3):500–16.
[89] Ravenelle RM, et al. Stability of zeolites in hot liquid water. J Phys Chem C 2010;114(46):19582–95.
[90] Hedlund J, Jareman F, Bons AJ, Anthonis M. A masking technique for high quality MFI membranes. J Memb Sci 2003;222(1–2):63–179.
[91] Lai R, Gavalas GR. Surface seeding in ZSM-5 membrane preparation. Ind Eng Chem Res 1998;37(11):4275–83.
[92] Sato K, Sugimoto K, Sekine Y, Takada M, Matsukata M, Nakane T. Application of FAU-type zeolite membranes to vapor/gas separation under high pressure and high temperature up to 5 MPa and 180 °C. Microporous Mesoporous Mater 2007;101(1-2):312–8.
[93] Piera E, et al. Synthesis, characterization and separation properties of a composite mordenite/ZSM-5/chabazite hydrophilic membrane. J Memb Sci 1998;149(1):99–114.
[94] Aoki K, Kusakabe K, Morooka S. Gas permeation properties of A-type zeolite membrane formed on porous substrate by hydrothermal synthesis. J Memb Sci 1998;141(2):197–205.
[95] Aoki K, Kusakabe K, Morooka S. Separation of gases with an A-type zeolite membrane. Ind Eng Chem Res 2000;39(7):2245–51.
[96] Algieri C, Comite A, Capannelli G. Zeolite membrane reactors. Handbook of Membrane Reactors 2013;1:245–70.
[97] C. Tellez and M. Menendez, "Zeolite membrane reactors", Membrane for Membrane Reactors, 2011, Chapter 8: 243-273.
[98] Lee SM, et al. Structure, stability and permeation properties of NaA zeolite membranes for H2O/H2 and CH3OH/H2 separations. J Eur Ceram Soc 2018;38(1):211–9.
[99] Sea B, Lee KH. Methanol synthesis from carbon dioxide and hydrogen using a ceramic membrane reactor. React Kinet Catal Lett 2003;80(1):33–8.
[100] R. Raso et al., "Zeolite membranes: Comparison in the separation of H2O/H2/CO2 mixtures and test of a reactor for CO2 hydrogenation to methanol," Catal. Today, 2021, 364, no. September 2019, pp. 270–275.
[101] Sawamura KI, Shirai T, Takada M, Sekine Y, Kikuchi E, Matsukata M. Selective permeation and separation of steam from water-methanol-hydrogen gas mixtures through mordenite membrane. Catal Today 2008;132(1–4):182–7.
[102] Salomón MA, Coronas J, Menéndez M, Santamaría J. Synthesis of MTBE in zeolite membrane reactors. Appl Catal A Gen 2000;200(1):201–10.
[103] Gascon J, Kapteijn F, Zornoza B, Sebastián V, Casado C, Coronas J. Practical approach to zeolitic membranes and coatings: State of the art, opportunities, barriers, and future perspectives. Chem Mater 2012;24(15):2829–44.
[104] Menendez M, Piera E, Coronas J, Santamaría J. Zeolite membrane reactor for the production of methanol and other alcohols form synthesis gas. Oepm 1999;2 164544:1–6.
[105] Rezai SAS, Lindmark J, Andersson C, Jareman F, Möller K, Hedlund J. Water/hydrogen/hexane multicomponent selectivity of thin MFI membranes with different Si/Al ratios. Microporous Mesoporous Mater 2008;108(1–3):136–42.
[106] T. Tomita, R. U. S. A. Data, P. Examiner, and J. M. Greene, "Method of dehydration. dehydrating apparatus and membrane reactor", United States Patent No US-7819944-B2, Oct.26, 2010.
[107] Ismail AF, David LIB. A review on the latest development of carbon membranes for gas separation. J Memb Sci 2001;193(1):1–18.
[108] Fu S, Sanders ES, Kulkarni SS, Koros WJ. Carbon molecular sieve membrane structure-property relationships for four novel 6FDA based polyimide precursors. J Memb Sci 2015;487:60–73.
[109] Naberezhnyi D, Gölzhäuser A, Dementyev P. Water-Assisted Permeation of Gases in Carbon Nanomembranes. J Phys Chem Lett 2019;10(18):5598–601.
[110] Teixeira M, Campo MC, Pacheco Tanaka DA, Llosa Tanco MA, Magen C, Mendes A. Composite phenolic resin-based carbon molecular sieve membranes for gas separation. Carbon N Y 2011;49(13):4348–58.